THE JOURNAL OF PHYSICAL CHEMISTRY A

Article

pubs.acs.org/JPCA

Magnetic Superatoms in VLi_n (n = 1−13) Clusters: A First-Principles Prediction

Meng Zhang,[†] Jianfei Zhang,[†] Xiaojuan Feng,[†] Hongyu Zhang,[†] Lixia Zhao,[†] Youhua Luo,*[,†] and Wei Cao*[,‡]

[†]Department of Physics, East China University of Science and Technology, Shanghai 200237, China

[‡]Department of Physics, University of Oulu, P.O. Box 3000, Oulu FIN-90014, Finland

ABSTRACT: We demonstrated a first-principles investigation to search for magnetic superatoms in the vanadium-doped lithium clusters VLi_n (n = 1−13). The stabilities of VLi_n clusters were determined through geometrical and electronic optimizations. It is found that the growth pattern of VLi_n in 3-space follows adding a Li atom capped on VLi_{n-1} clusters. All doped clusters show larger relative binding energies compared with pure Li_{n+1} partners and display tunable magnetic properties. When n = 8−13, the VLi_n clusters adopt a cage-like structure with an endohedral V atom and are identified as superatoms with their magnetic moments successively decreasing from 5 to 0 μ_B. The isolated VLi_8 superatom is emphasized due to its robust magnetic moment as well as high structural and chemical stability analogue of a single Mn^{2+} ion. Molecular orbitals analysis shows that VLi_8 has an electronic configuration of $1S^21P^61D^5$, exhibiting Hund's filling rule of maximizing the spin-like atoms. Electronic shell structures of $1S^2$ and $1P^6$ are virtually unchanged in Li_9 cluster as the V atom substitutes for the embedded Li atom, indicating that the electron-shell-closing model is valid for explaining its structures and stabilities. The results show that the tailored magnetic building blocks for nanomaterials can be formed by seeding magnetic dopants into alkali metal cluster cages.

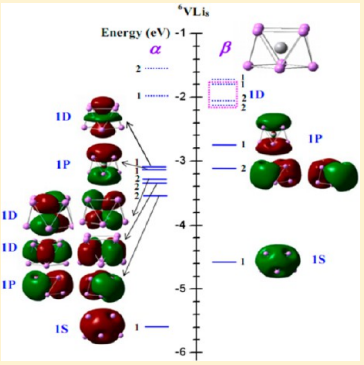

1. INTRODUCTION

Since the pioneering finding of the celebrated C_{60},[1] one of the major goals of cluster science has been dedicated to discovering highly stable clusters with unique properties for the purpose of building blocks in novel nanomaterials. Metal clusters often show different physical and chemical properties from their bulk counterparts yet drawing tremendous attention due to their unique optical properties, magnetic properties, as well as catalytic reactivities.[2−4] Particularly, newly developed cluster superatoms consisting of specific atoms that share electrons but mimicking chemical behaviors of other elements have been studied extensively in recent years.[5−13] Superatoms with unusual properties give a new perspective on the periodic table and provide an unprecedented ability to design novel materials. Bergeron et al. reported that Al_{13} and Al_{14} are halogen-like and alkaline-earth-like superatoms in the $Al_{13}I_n^-$ (n = 1−12) and Al_{14} I_n^- (n = 1−11) complexes, respectively.[14] It was proposed later by Walter et al. that the superatom concept can also be extended to thiolate (RS)-coordinated gold clusters such as $Au_{25}(SR)_{18}^-$ and $Au_{102}(SR)_{44}$.[15] The electronic shells in superatoms can be grouped into shells 1S, 1P, 1D, 2S, ... by examining the nodal shapes of their molecular orbitals (MOs), much in the same way as that in atoms (s, p, d, f, ...), where the uppercase letters are used to distinguish them from atomic orbitals that are generally labeled by lowercase symbols.

Different from a single atom whose orbital fillings follow the Hund's rule, clusters can undergo atomic deformations to break degeneracy in electronic states through Jahn−Teller effects. Early studies of cluster superatoms were within the so-called jellium sphere framework.[16] Collections of atoms in a compact spherical arrangement species consist of filled electronic shells, such as the cluster Al_{13}^- with the magic number of the 40 valence electrons.[9] All electrons in such stable electronic configurations are paired, resulting in nonmagnetism of the superatoms. In 2009, Khanna and co-workers reported that encapsulating a vanadium atom into a cage of eight cesium atoms could create a stable supershell of electrons and prevent the vanadium atom's unpaired electrons from reacting with other atoms and maintain its magnetism. The VCs_8 cluster has a magnetic moment of 5 μ_B, the same as a manganese atom.[17] Khanna et al. pointed out that one way to stabilize magnetic superatoms is to introduce an additional transition metal (TM) atom, which can breed magnetism through its specific orbital configuration that hybridizes with the superatom and stabilizes the magnetic state. Later, they extended their investigations to other alkali metals and alkaline earth metal systems doped with 3d TM dopants. The bimetallic clusters VNa_8, $FeCa_8$, $CrSr_9$, $MnCa_9$, $ScNa_{12}$, ScK_{12}, and $ScCs_{12}$ are also considered magnetic superatoms with large spin.[18−22] This research opened a new path of infusing magnetic character in otherwise nonmagnetic elements through controlled association with a single magnetic atom.

Lithium is the first alkali metal that can be considered as an ideal prototype for simple metals and presents a good starting

Received: October 23, 2013
Revised: November 12, 2013
Published: November 13, 2013

   dx.doi.org/10.1021/jp410489g | J. Phys. Chem. A 2013, 117, 13025−13036

Table 1. Calculated Bond Distance d (Å), Vibrational Frequency ω_e (cm^{-1}), Average Binding Energies Per Atom E_b (eV), and Ionization Potential IP (eV) of the Li_2, Li_2^-, and Li_3 Clusters Optimized Using Different Density Functional Methods

	Li_2				Li_2^-		Li_3
methods	d	ω_e	E_b	IP	d	ω_e	IP
BP	2.74	432	0.40	4.93	3.12	276.9	4.05
BLYP	2.70	333.6	0.47	4.99	3.14	244.7	3.88
PBE	2.70	306.2	0.46	5.03	3.10	282.8	4.06
PW91	2.70	332	0.48	5.12	3.09	275.9	4.09
expt.[23−26]	2.67	351.4	0.52	5.14	3.09 ± 0.015	232 ± 35	4.08

point for theoretical understanding of metal clusters. Moreover, lithium has received intense research interest due to its high power and capacity for rechargeable lithium batteries and high capacity for hydrogen storage in lithium materials. Lithium and lithium-based clusters continue to attract attention because of their interesting physical and chemical properties. During the past 2 decades, pure lithium clusters in the small size range have been assigned through experimental[23−27] and theoretical studies[28−39] by various density functional theory (DFT) and ab initio methods. In 2013, using Li clusters as a test case, Cheng et al. proposed a new concept for bonding between superatoms and gave more generalized insight to the stability of nonspherical clusters. They found that Li_{14}, Li_{10}, and Li_8 clusters are analogues to F_2, N_2, and CH_4 molecules, respectively.[40] In addition, a considerable amount of work has been carried out on lithium clusters doped with an impurity atom, which can lead to fundamental changes in geometries, energy properties, and the bonding nature of lithium clusters. For example, the heterogeneous XLi_n clusters doped with group IA elements with X = Na and K,[41−43] group IIA elements including beryllium $BeLi_n$[44] and magnesium $MgLi_n$,[45] group IIIA elements such as BLi_n[46−52] and $AlLi_n$,[53−62] and group IVA with X = C, Si, Ge, and Sn[63−73] have extensively been studied by many groups. These studies focused on the investigations of s-block and p-block element doped small lithium clusters; however, there have been few studies on lithium clusters doped with transition elements.

Beyond the above studies based on alkali metal matrixes, however, research of employing lithium clusters as superatom doping hosts has been carried out far less. Taking the above research progress and importance of TM-doped alkali metal clusters into account, we performed a first-principles study of the vanadium-doped lithium clusters VLi_n (n = 1−13) to systematically explore their structural evolution and properties. Because the lithium has the s^1 valence configuration, similar to cesium, it is expected that the aggregation of lithium clusters and TM elements with the partially filled d shells will probably result in magnetic superatoms. We started our explorations on the size-dependent growth behavior related to the stability of the bimetallic VLi_n clusters, and then, we investigate the electronic and magnetic properties of VLi_n in comparison to pure lithium clusters. Following the research focuses in the formation of superatoms in VLi_n clusters, we found the highly stable cluster VLi_8 as a magnetic superatom candidate with 5 μ_B, meanwhile consisting of closed shells of eight paired electrons and five unpaired electrons occupying the $1D_{xy}$ $1D_{x^2-y^2}$, $1D_{xz}$, $1D_{yz}$, and $1D_{z^2}$ levels. Moreover, it demonstrates that the VLi_n clusters from the size of n = 8 to 13 with cage-like structures all have the superatomic orbitals. The magnetic properties of the various 3d TM atom doped Li_8 cages are also discussed in the context. We hope that our work will add new types of superatoms in alkali metal clusters.

2. COMPUTATIONAL METHODS

Calculations in this work were performed by using DFT implemented in the DMOL3 program.[74] Relativistic calculations were carried out with scalar relativistic corrections to valence orbitals relevant to atomic bonding properties via a local pseudopotential (VPSR). All-electron spin-unrestricted calculations with double-numerical basis sets including d polarization functions (DNP) were employed. The quality of the self-consistent field (SCF) convergence tolerance was set as "fine" with a convergence criterion of 1×10^{-5} Hartree on the total energy and electron density, 2×10^{-3} Hartree/Å on the gradient, and 5×10^{-3} Å on the displacement in our calculations. Harmonic vibrational frequencies were computed to confirm that the low-energy isomers are true minima. There is no imaginary frequency for structures presented here. In addition, for geometry optimization of each isomer, the spin multiplicities (SMs) were considered to be at least 1, 3, 5, 7, and 9 for even-electron clusters and 2, 4, 6, 8, and 10 for odd-electron clusters. If the total energy decreases with increasing SM, we will consider a higher spin state until the energy minimum with respect to the SM is reached. In the present work, we chose the initial structures of VLi_n clusters by two methods, as follows: First, the basin-hopping global optimization method was employed to produce a large number of isomers for further DFT optimization.[75,76] Second, the low-lying structures were obtained by placing the V atom on each possible site of the Li_n host clusters randomly as well as by substituting one Li by a V atom in the Li_{n+1} cluster.

To choose the most valid gradient-corrected exchange−correlation functionals for the lithium clusters system, we performed calculations on Li_2, Li_2^-, and Li_3 clusters with four popular functionals, namely, Becke's 1988 exchange functional and the correlation functional of Perdew (BP86),[77] Becke's 1988 exchange functional and the correlation functional of Lee, Yang, and Parr (BLYP),[78] the 1996 exchange functional of Perdew, Burke, and Ernzerhof (PBE),[79] and Perdew and Wang's 1991 exchange and correlation functional (PW91).[80] The results are listed in Table 1. It can be seen from Table 1 that the calculated bond length, average binding energies, and ionization potential based on the PW91 method are in best agreement with the experimental values. This indicates that the functional PW91 is confirmed to yield the most reliable results. Therefore, we selected the functional PW91 for most calculations carried out in this study.

3. RESULTS AND DISCUSSION

Aiming for the discovery of stable superatoms in the present system, we dug thoroughly through the whole sequence of V-doped Li_n (n = 1−13) clusters. The VLi_n cluster growth pattern was first investigated. Relative stabilities were justified afterward through their electronic structures. Magnetic properties of the

dx.doi.org/10.1021/jp410489g | J. Phys. Chem. A 2013, 117, 13025−13036

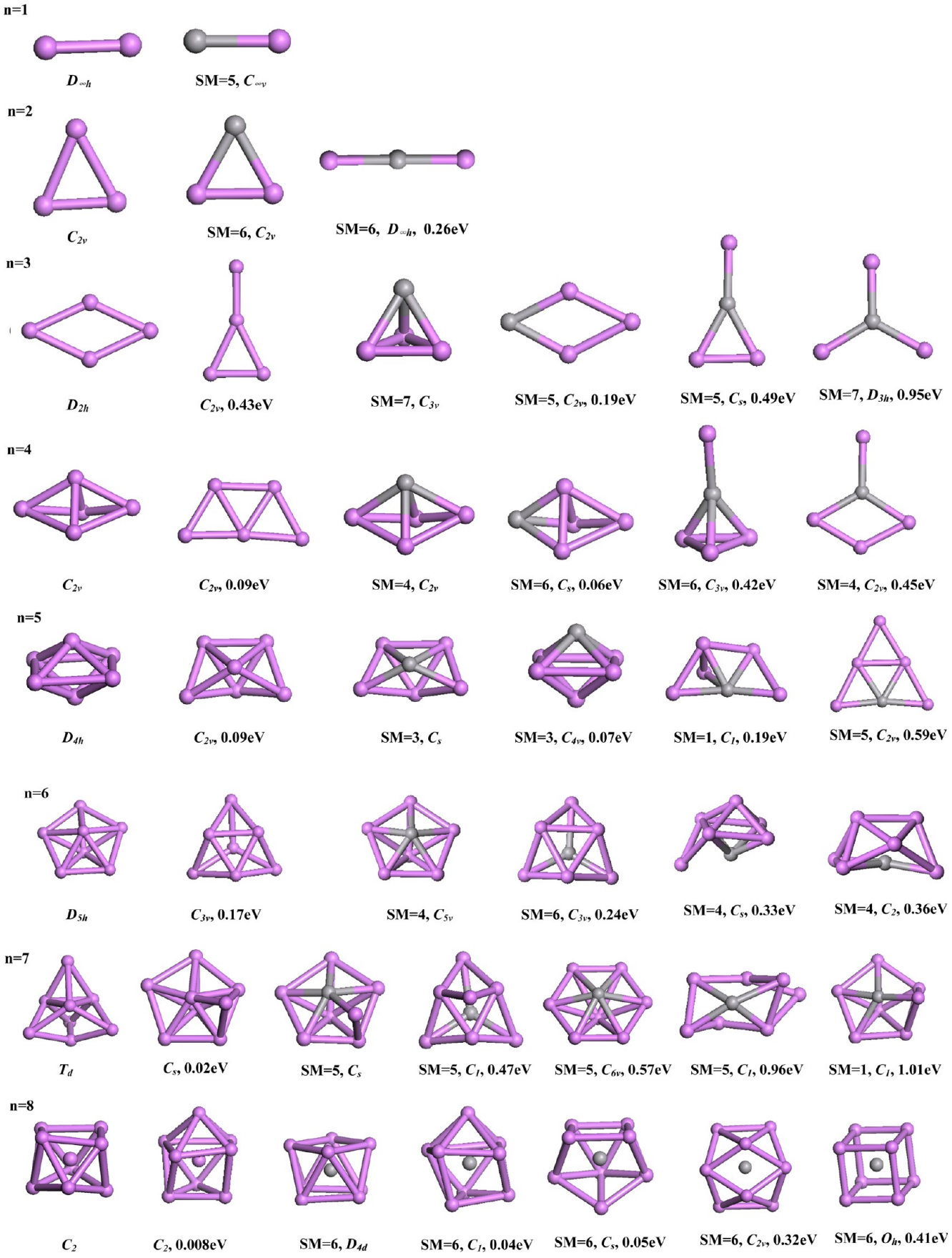

Figure 1. continued

dx.doi.org/10.1021/jp410489g | J. Phys. Chem. A 2013, 117, 13025−13036

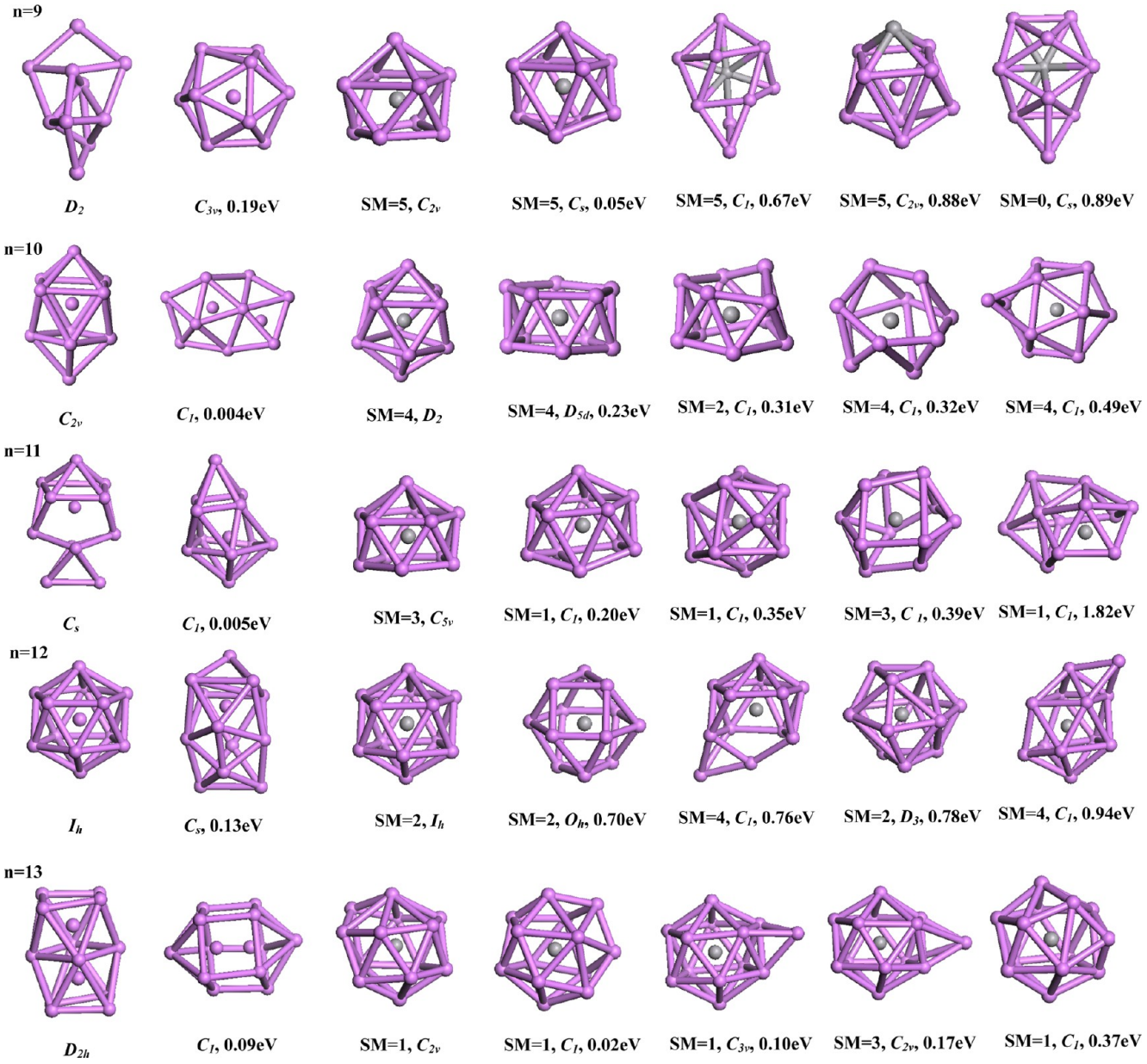

Figure 1. The lowest-energy structures and low-lying isomers with the spin multiplicities (SMs) and relative energies (in eV) of VLi_n (n = 1−13) clusters. The ground-state and metastable geometries of the corresponding bare Li_{n+1} clusters are also given on the left. See Table 2 for the corresponding energetic and structural information. The V atom is represented by the gray sphere.

stable binary clusters were discussed subsequently. Taking their magnetic and stable characteristics into considerations, a distinctive magnetic superatom was found with a potential extension to other similar TM-doped Li_n clusters. Thus, the present section is subdivided into four parts, with each part describing the above-mentioned steps.

3.1. Geometric Structure. We considered extensive two-dimensional (2D) and three-dimensional (3D) structures to determine the lowest-energy geometries for each bimetallic VLi_n cluster. Many stable isomers were obtained. The lowest-energy structures together with some low-lying isomers of VLi_n and corresponding bare Li_{n+1} (n = 1−13) clusters are shown in Figure 1. The symmetries, SMs, and the differences of the total binding energies between an isomer and the lowest-energy structure optimized with PW91/VPSR are also listed below each isomer in Figure 1. The lowest-energy geometries of pure Li_{n+1} clusters from our optimized results are in agreement with the results reported in the literature.[28−33,38−40] The calculated ionization potential (IP) of the pure Li_3 cluster with a planar triangle structure in the present work is in good agreement with the result of the experiment (see Table 1).[23] For pure lithium clusters, the 2D → 3D transition is found to occur in Li_5 in our calculations, in accordance with the previous calculations of Tai et al. using the coupled-cluster theory CCSD(T)/complete basis set (CBS) methods based on DFT.[51,52] Moreover, the structural transition from the compact to hollow-cage structure is found at n = 8, which is in agreement with the results of Yepes et al.[29] The optimized geometries reveal that VLi_n clusters prefer 3D structures with the successive lithium atoms surrounding the central vanadium site. A single Li-atom-capped structure of the VLi_{n-1} cluster is a dominant growth pattern. The structure evolves toward a compact

dx.doi.org/10.1021/jp410489g | J. Phys. Chem. A 2013, 117, 13025−13036

Table 2. Geometrical Structures with the Symmetry Type, the SM, the Binding Energy (E_b) Per Atom, the Fragmentation Energy (E_f), and the HOMO−LUMO Energy Gap E_{gap} of VLi_n Clusters and the Corresponding Bare Li_{n+1} Clusters (n = 1−13) for the Lowest-Energy Structures[a]

pure Li_n						VLi_n					
cluster	symmetry	E_b (eV)	E_b (expt.)	E_f (eV)	E_{gap}(eV)	cluster	symmetry	SM	E_b (eV)	E_f (eV)	E_{gap}(eV)
Li_2	$D_{\infty h}$	0.48	0.53	0.95	1.491	VLi	$C_{\infty v}$	5	0.70	1.41	0.468
Li_3	C_{2v}	0.54	0.50	0.67	0.494	VLi_2	$D_{\infty h}$	6	0.81	1.02	0.308
Li_4	D_{2h}	0.72	0.63	1.26	0.976	VLi_3	C_{3v}	7	0.95	1.36	0.756
Li_5	C_{2v}	0.79	0.78	1.07	0.338	VLi_4	C_{2v}	4	1.02	1.31	0.510
Li_6	D_{4h}	0.89	0.88	1.42	0.738	VLi_5	C_s	3	1.08	1.39	0.604
Li_7	D_{5h}	0.98	0.91	1.51	0.562	VLi_6	C_{5v}	4	1.18	1.76	0.374
Li_8	T_d	1.01	0.95	1.22	0.976	VLi_7	C_s	5	1.21	1.40	0.514
Li_9	C_2	1.01		1.02	0.390	VLi_8	D_{4d}	6	1.28	1.80	0.779
Li_{10}	D_2	1.05		1.42	0.875	VLi_9	C_{2v}	5	1.30	1.51	0.328
Li_{11}	C_{2v}	1.06		1.16	0.416	VLi_{10}	D_2	4	1.32	1.55	0.309
Li_{12}	C_s	1.09		1.42	0.660	VLi_{11}	C_{5v}	3	1.34	1.53	0.196
Li_{13}	I_h	1.12		1.42	0.524	VLi_{12}	I_h	2	1.38	1.86	0.196
Li_{14}	D_{2h}	1.13		1.32	0.842	VLi_{13}	C_{2v}	1	1.36	1.16	0.519

[a]For the sake of comparison, the experimental values (ref 26) of E_b of the bare Li_{n+1} clusters (n = 1−7) are given.

icosahedral shape with the increase of lithium atom number. It is found that the SMs for the low-lying isomers of the VLi_n clusters are not only size-dependent but also structure-dependent, as shown in Figure 1.

The ground state of diatomic VLi exhibits a $C_{\infty v}$ symmetry. For the triatomic VLi_2 cluster, the angular isomer with the C_{2v} symmetry, which relates to the lowest-energy structure of the Li_3 cluster, is found to be the most stable structure. The linear configuration in which the Li atom occupies the central position with the $D_{\infty h}$ symmetry is 0.26 eV higher in energy than the triangle isomer. Starting at the size of n = 3, the lowest-energy structures of VLi_n clusters begin to show the appearance of 3D geometries. A triangular pyramid with C_{3v} symmetry is the most stable structure for VLi_3. The 2D C_{2v} rhombic form and the Y-shaped planar geometry lie 0.19 and 0.49 eV higher in energy, respectively. The most stable isomer of the VLi_4 cluster has a triangular bipyramidal structure with a C_{2v} point group. The second isomer of the VLi_4 cluster in which the V atom lies at the corner of the bipyramid is 0.06 eV higher in energy. The lowest-energy structure of VLi_5 is obtained by subsequent addition of one Li atom to the VLi_4 structure. The squared pyramidal with C_{4v} is calculated to be only 0.07 eV less stable than the C_s structure. Similar to the configuration of the ground-state Li_7 cluster, a pentagonal bipyramid (C_{5v}) with the impurity V atom at one of the apexes is the lowest-energy structure for VLi_6 clusters. VLi_7 can be viewed as adding a Li atom to the pentagonal bipyramid of VLi_6 by distortion.

The number of isomers for VLi_n is increasing as successive Li atoms are added to a V atom. From n = 8 to 13, the lithium atoms adopt a cage-like structure, and the endohedral V atom occupies at the center site in the ground-state structures. The isomers with the V atom at a surface site are all found to be higher in energy. The VLi_8 cluster in D_{4d} symmetry is derived from the lowest-energy structure of pure Li_9 with a square antiprism where the dopant V atom is sitting in the center. This structure is similar to other superatoms such as VCs_8, VNa_8, and $FeCa_8$ clusters.[17,20] The second and third lowest-energy isomers are very close in energy and have a large structural distortion relative to the most stable structure. The higher-symmetry O_h cubic structure is 0.41 eV higher than the square antiprism isomer, and from this cluster onward, the V atom is seen to be encapsulated in a Li cage, as shown in Figure 1. VLi_9 can be viewed as a capped square antiprism of a VLi_8 cluster. This trend of capping continues up to n = 13. In addition, the tendency for the formation of a pentagonal ring is also clear. The lowest-energy structure of VLi_{12} is the icosahedron with perfect I_h symmetry, in which the V atom is located in the center of the Li_{12} cage. The octahedral isomer with O_h symmetry is 0.70 eV higher in energy than the icosahedral isomer.

It should be noted that the geometrical structures of TM impurity V-atom-doped Au_n (n = 1−14) clusters were systematically investigated by Nhat et al. using BP86/cc-pVTZ-PP calculations.[81] Although Au and Li have similar outermost shell electronic structures, namely, one s electron, the structures of VAu_n clusters obtained by Nhat et al. are very different from the corresponding VLi_n clusters. This is because lithium is the lightest metal, while gold is an element whose unique properties are strongly influenced by relativistic effects. The strong relativistic effect in gold leads to a reduced 5d−6s energy gap and strong s−d hybridization. For TM impurities in a nonmagnetic host, the interaction of the impurity d states with the different host metal plays a crucial role in determining the structures and properties of the clusters.

3.2. Relative Stabilities. Table 2 gives various structural and energetic characteristics for the lowest-energy structures of VLi_n clusters and the corresponding bare Li_{n+1} clusters (n = 1−13). To further analyze the stability of clusters, we calculated the average binding energy (E_b) per atom of VLi_n, which is defined as the difference between the energy sum of all of the free atoms constituting the cluster and the total energy of the cluster using the following formula:

$$E_b(VLi_n) = \frac{[nE(Li) + E(V) - E(VLi_n)]}{(n+1)} \quad (1)$$

The fragmentation energy (E_f) of the lowest-energy structure is also discussed, which is defined as the energy that is released when a Li atom is separated from these clusters calculated using the equation

$$E_f(VLi_n) = [E(VLi_{n-1}) + E(Li) - E(VLi_n)] \quad (2)$$

In the above equation, $E(VLi_n)$ and $E(VLi_{n-1})$ represent the energy of the lowest-energy structures of VLi_n and VLi_{n-1}

dx.doi.org/10.1021/jp410489g | J. Phys. Chem. A 2013, 117, 13025−13036

clusters, respectively. The average binding energies per atom of the pure Li_{n+1} clusters are in good agreement with the available experimental results, as Table 2 shows.[26] It can be seen from Table 2 that the E_b for the ground state of VLi_n (n = 1−13) clusters is significantly higher than that of the corresponding pure Li_{n+1}. This indicates that doping with the V atom, which has the partially filled d shells, can enhance the stabilities of the Li_n clusters. Figure 2 shows the E_b and E_f of the VLi_n clusters

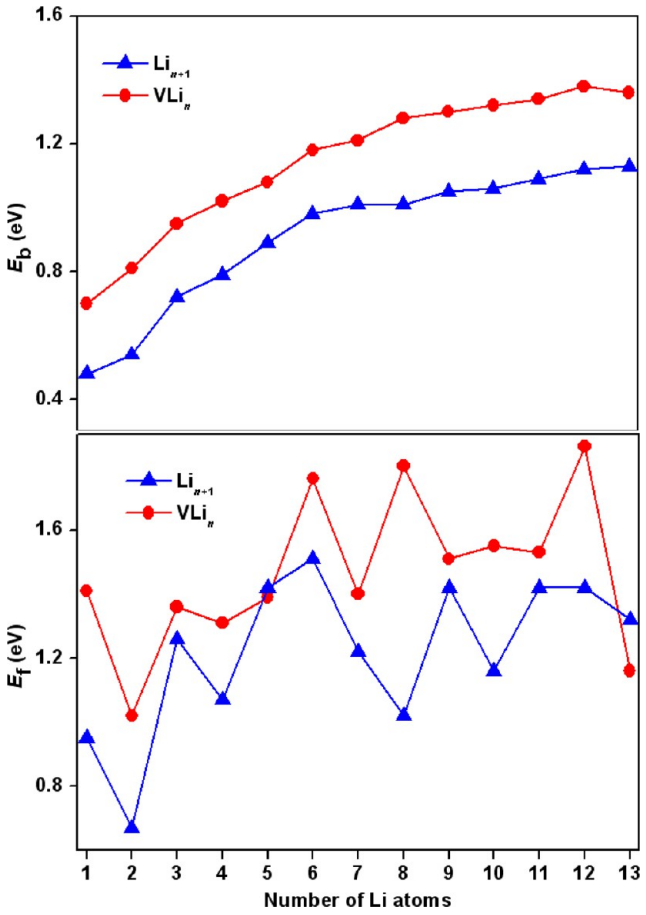

Figure 2. Comparison of the average binding energies per atom (E_b) and fragmentation energies (E_f) of the VLi_n and bare Li_{n+1} clusters (n = 1−13) for the lowest-energy structures.

for the lowest-energy structures as a function of the number of Li atoms. As seen from the Figure 2, the binding energy of VLi_n clusters increases monotonically with cluster size. However, three conspicuous maxima of fragmentation energies for VLi_n clusters are found at n = 6, 8, and 12 in Figure 2, indicating that VLi_6, VLi_8, and VLi_{12} clusters possess relatively higher stability than their respective neighbors.

The energy gap (E_{gap}) between the highest occupied molecular orbital (HOMO) and the lowest unoccupied molecular orbital (LUMO) is another useful quantity for examining the kinetic stability of small clusters. A large energy gap corresponds to a high energy required for electron excitation. We plotted the energy gap of the most stable VLi_n and Li_{n+1} clusters in Figure 3. There are clear odd−even oscillations in the energy gap spectrum of the pure Li_{n+1} clusters. We found that the E_{gap} of VLi_n clusters varies significantly with size, and VLi_8 exhibits a particularly large E_{gap} with 0.779 eV. Figure 3 shows a distinct maximum at VLi_8

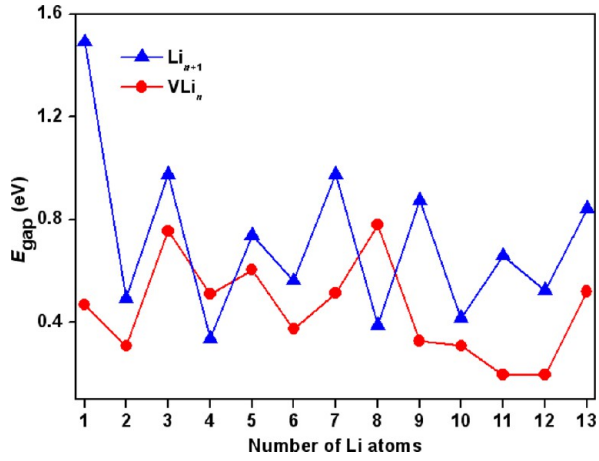

Figure 3. The HOMO−LUMO energy gap (E_{gap}) of the VLi_n and bare Li_{n+1} clusters (n = 1−13) for the lowest-energy structures.

clusters, larger than the values of other clusters, indicating that VLi_8 is relatively more stable in the electronic structure.

Mulliken population analysis was performed for the lowest-energy structures, and the atomic charge on the V atom of VLi_n clusters is given in Table 3 and plotted in Figure 4. The charge on the impurity V atom, ranging from −0.167 to 0.217 au, clearly shows that there are obvious charge transfers between V and Li atoms. In small clusters from VLi to VLi_5, charge transfers occur from the Li to V atom due to a larger electronegativity of the V. However, charge transfers reverse as successive Li atoms are added. The impurity V atom is likely to lose its valence electrons, and the host Li has a negative charge. The VLi_8 cluster with a vanadium atom surrounded by a square antiprism of eight lithium atoms has the largest charge transfers among these clusters, which is responsible for the higher stability of the VLi_8 cluster than its neighbors due to ionic-like bonding of the V−Li interaction through the charge transfers. To have a better view of the interactions between V and Li atoms, the deformation electron density (DED) of the bare Li_9 and VLi_8 clusters for the lowest-energy structures as the example is plotted in Figure 5a. The DED is defined as the total charge density of a cluster with the density of the isolated atoms subtracted. The blue area indicates electron accumulation when atoms form a cluster. From Figure 5a, we can see that the DED distributes not only surrounding the V and Li atoms but also surrounding the intervals between Li and V atoms in the VLi_8 cluster, which shows some covalent character in the V−Li bonds. In comparison to the pure Li_9 cluster (see Figure 5a), when the V atom substitutes one Li atom in the square antiprism structure, the electron accumulations of V−Li atoms and Li−Li atoms show a marked increase. This verifies that the strong interaction between the V and Li exists in VLi_8 and results in the high stability of the structure.

3.3. Magnetic Properties. Different from a single atom, the filling of the electronic orbitals in clusters does not follow Hund's rule of maximizing the spin because the structural distortions in small clusters can remove the degeneracies in electronic shells and stabilize the clusters via the Jahn−Teller effect.[82] This results in superatoms with pairs of electrons favoring nonmagnetic character. In what follows, we will examine the variation in the magnetic moment of VLi_n clusters as successive Li atoms are added. The local magnetic moments on 3d, 4s, and 4p states of the V and Li atoms and the total magnetic moment of the ground-state VLi_n clusters are listed in

dx.doi.org/10.1021/jp410489g | J. Phys. Chem. A 2013, 117, 13025−13036

Table 3. Mulliken Charge (au) on the V Atom, Local Magnetic Moment (μ_B) of the Guest V and Host Li Atoms, and Total Magnetic Moment of VLi_n (n = 1−13) Clusters for the Lowest-Energy Structures

		moment (μ_B)					
			V				
system	charge (au)	Li_n	3d	4s	4p	local	total
VLi	−0.106	−0.205	3.809	0.391	0.005	4.205	4
VLi_2	−0.089	0.709	3.746	0.489	0.056	4.291	5
VLi_3	−0.122	1.429	3.932	0.524	0.115	4.571	6
VLi_4	−0.167	−0.662	3.759	−0.157	0.058	3.662	3
VLi_5	−0.112	−1.636	3.728	−0.120	0.028	3.636	2
VLi_6	0.027	0.607	3.534	−0.055	0.129	3.607	3
VLi_7	0.101	−0.023	3.673	0.140	0.209	4.023	4
VLi_8	0.217	0.568	3.965	0.218	0.250	4.432	5
VLi_9	0.180	−0.091	3.622	0.227	0.242	4.091	4
VLi_{10}	0.155	−0.876	3.469	0.173	0.233	3.876	3
VLi_{11}	0.195	−1.646	3.187	0.226	0.233	3.646	2
VLi_{12}	0.188	−2.302	2.887	0.199	0.217	3.302	1
VLi_{13}	0.174	0	0	0	0	0	0

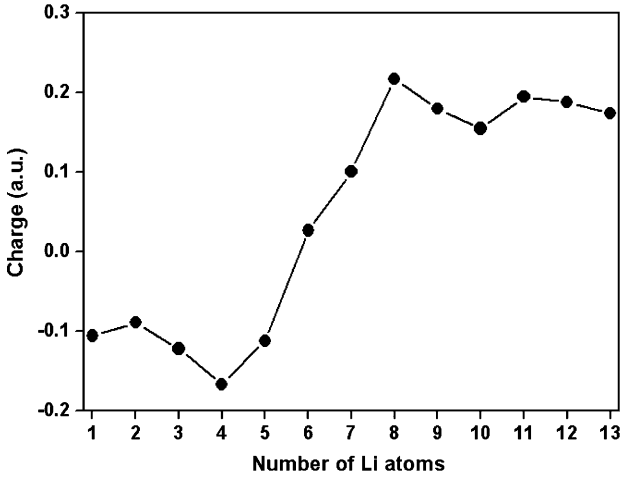

Figure 4. The atomic charge (au) on the V atom of the VLi_n clusters (n = 1−13) for the lowest-energy structures.

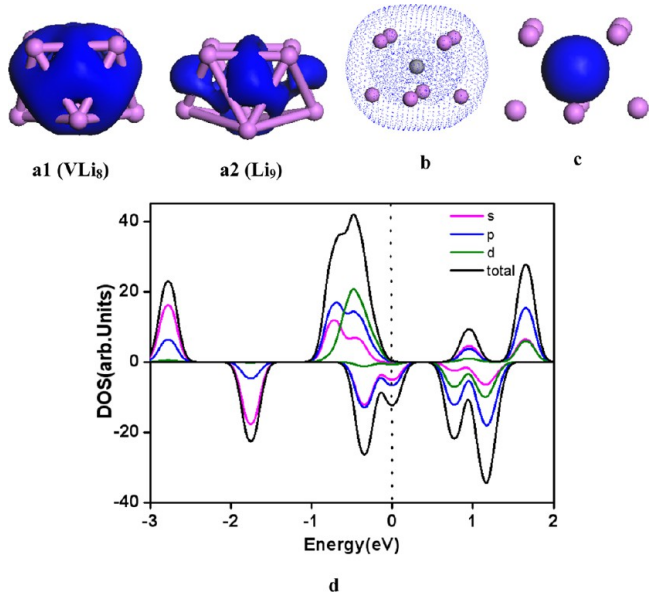

Figure 5. The DED (a), total electron density (b), net spin electron density (c), and electronic density of states (DOS) (d) of the VLi_8 cluster for the lowest-energy structure. The surface isovalue for MO plotting is 0.3 e/Å^3. The DOS is obtained by Gaussian extension applied to the eigenvalues, and the broadening width parameter is chosen to be 0.1 eV. Spin-up (positive) and spin-down (negative) densities are given, and the dashed lines indicate the location of the HOMO level.

Table 3 and plotted in Figure 6. The total magnetic moment of bare Li_{n+1} clusters shows a pronounced odd−even alternation (0 and 1 μ_B, respectively) with the number of Li atoms. A single V atom has three unpaired electrons with an atomic configuration of $3d^34s^2$. When a V atom with the partially filled 3d orbital is doped into Li_n clusters, the formed VLi_n clusters generate a diversiform magnetic moment, varying from 0 to 6 μ_B with the different cluster sizes. It is found that the VLi_8 has the robust magnetic moment of 5 μ_B. Figure 6 displays that from the size of n = 5 to 13, the magnetic moment of VLi_n clusters increases with Li number and reaches its maximum at VLi_8 and then decreases gradually to 0 μ_B at the size of n = 13. Consequently, the various styles of magnetic moments in VLi_n clusters suggest that nonmagnetic Li_n clusters can serve as flexible hosts to enhance, protect, or reduce the spins of the dopant magnetic atom, which has potential applications in new nanomaterials with tunable magnetic properties.

Mulliken population analysis shows that the total magnetic moment of the clusters is mainly localized in the V atom. A small amount of magnetic moment is found in host Li atoms, which show that the 3d V atom plays a decisive role in the magnetic moment of Li nanoclusters. This phenomenon can also be reflected from Figure 5b and c that although the total charge density of VLi_8 is extended over the entire cluster, the spin density is almost entirely located on the vanadium site. The magnetic moment of the V atom in the VLi_{13} cluster is fully quenched because this cluster attains an 18-electron shell closing. Except for VLi_{13}, the local magnetic moments contributed to by the 3d state electrons of V are about 2.887−3.965 μ_B in VLi_n (n = 1−12) clusters. The 4s and 4p subshells, which are nonmagnetic for a free V atom, provide a small contribution to the magnetic moments, as shown in Table 3. This may be ascribed to the internal charge transfer from the 4s and 4p orbitals to the 3d orbital and the hybridization between the d state and the s and p states. The partial density of states (PDOS) of the VLi_8 cluster in Figure 5d clarifies the

dx.doi.org/10.1021/jp410489g | J. Phys. Chem. A 2013, 117, 13025−13036

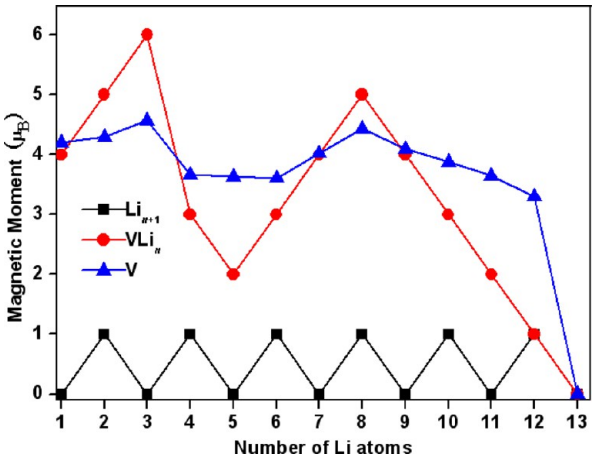

Figure 6. The local magnetic moment on the V and Li atoms and the total magnetic moment of the VLi_n clusters (n = 1−13) for the lowest-energy structures.

obvious hybridization between the atomic orbitals of the guest atom V (d orbital) and host atom Li (s orbital). Figure 5d shows that the shapes of the total density of states for the α electron (spin-up) and β electron (spin-down) are quite different in forming the magnetism of VLi_8 with 5 μ_B.

3.4. Magnetic Superatoms. On the basis of the above discussion, we note that VLi_8 is an isolated cluster with a high fragmentation energy of 1.80 eV, a big energy gap of 0.78 eV, a large charge transfer of 0.217 au, and a robust magnetic moment of 5 μ_B among these clusters. This indicates that VLi_8 has enhanced structural and chemical stability and large spin state, and it can be a candidate to magnetic superatoms. To identify the nature of orbitals, we present the MO and orbital energy level correlation diagram of the VLi_8 in Figure 7. The MO results of the pure Li_9 clusters are also depicted for comparison. The MO analysis was calculated with the PW91/LANL2DZ level in G09.[83] The VLi_8 cluster contains 13 valence electrons and does not correspond to a magic species with an 18-electron shell closing. However, the electronic configuration

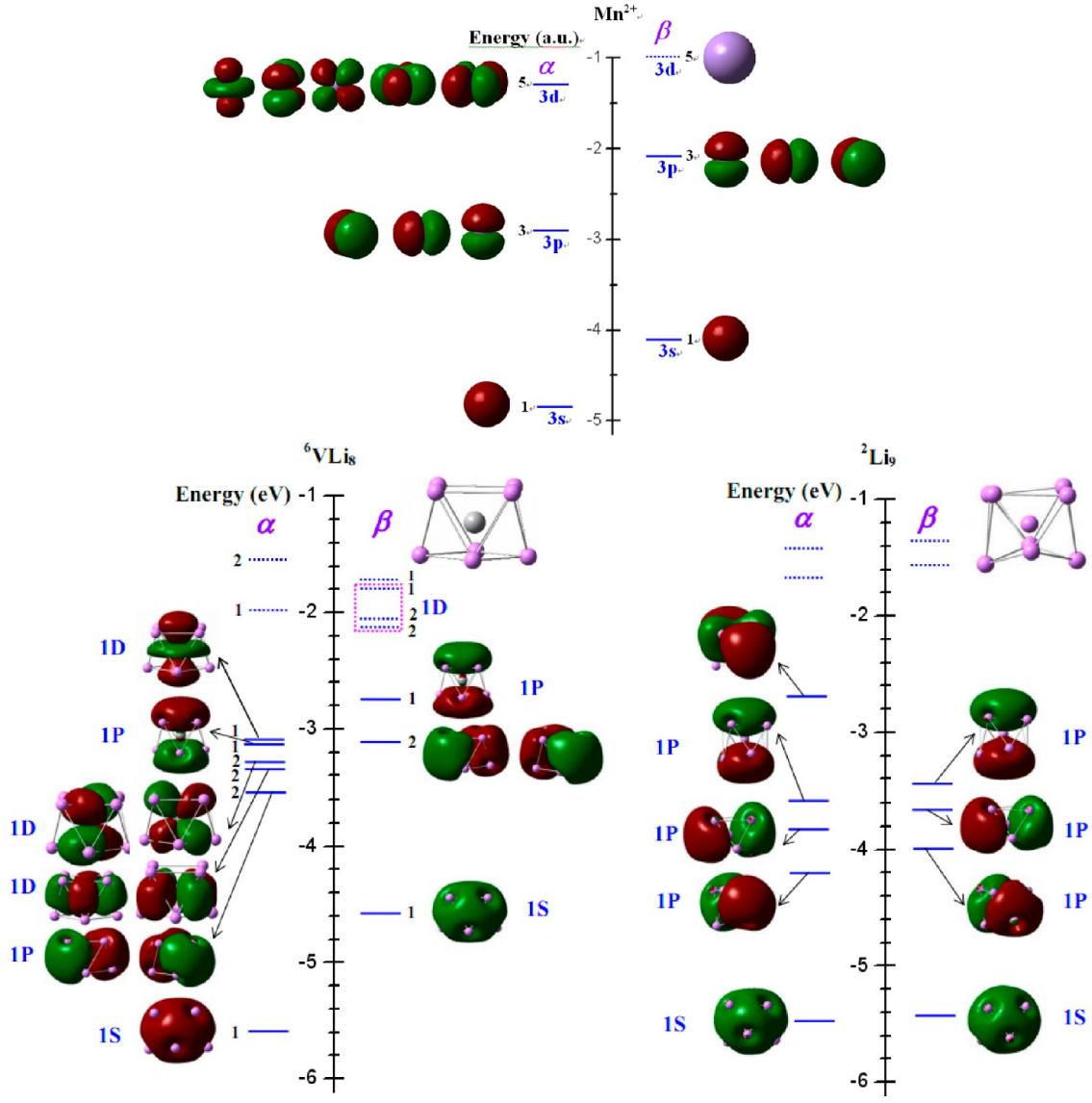

Figure 7. The MOs and MO energy level correlation diagrams of the VLi_8, Li_9, and single Mn^{2+} cation for the lowest-energy structures calculated with the PW91/LANL2DZ level in G09. Continuous lines correspond to the filled levels, and the dotted lines correspond to the unfilled states. For each level, the degeneracy is marked. The surface isovalue for MO plotting is 0.02 e/Å^3.

dx.doi.org/10.1021/jp410489g | J. Phys. Chem. A 2013, 117, 13025−13036

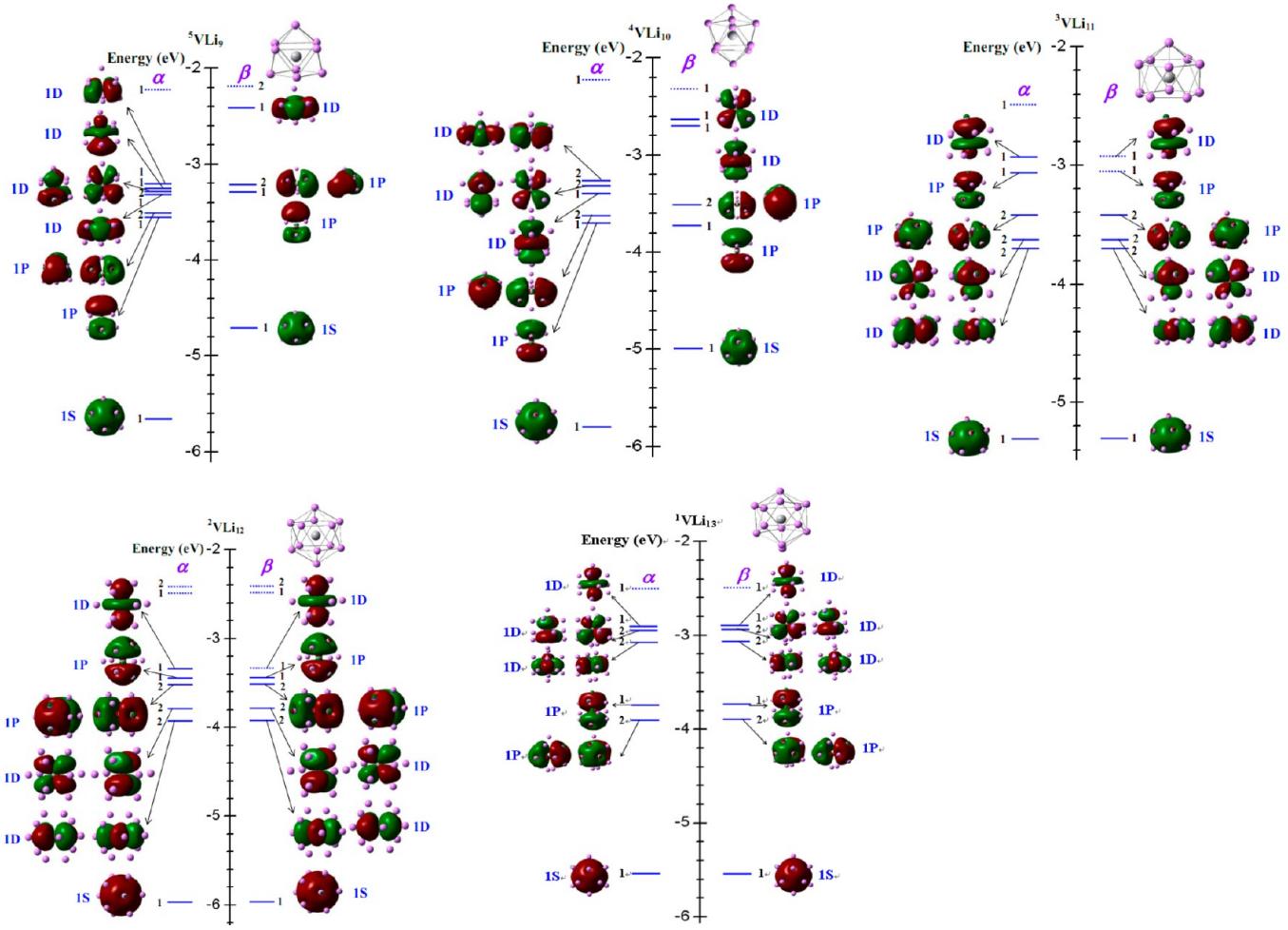

Figure 8. The MOs and MO energy level correlation diagrams of the VLi_n (n = 9−13) for the lowest-energy structures calculated with the PW91/LANL2DZ level in G09. The illustration is the same as that in Figure 7.

of VLi_8 can be considered as a jellium sphere. It consists of the five vanadium electrons in excess of the closed-shell eight-electron configuration, which contains the four orbitals in the 1S and 1P shells, each with an electron pair. The extra five electrons from the V atom are then placed singly into each of the five orbitals of the 1D shell so that they are all unpaired. Therefore, the VLi_8 cluster has a half-filled D subshell with a magnetic moment of 5 μ_B, and the remaining electrons form a filled shell of $1S^21P^6$ electrons, which leads to a stable species. Here, the VLi_8 cluster exhibits Hund's filling rule of maximizing the spin-like atoms. Figure 7 shows that the first two electrons occupy the lowest state, which is spread out over the whole VLi_8 cluster and has 1S superorbital character. The next majority states are two degenerate 1P states that have a $1P_x$ and $1P_y$ character, while the $1P_z$ state is pushed around 0.43 eV higher in energy as the VLi_8 cluster can be regarded as a compression of the spherical jellium in the z direction. The next higher energy orbitals above the 1P orbitals are 1D orbitals. The oblate shape of the cluster broke the degeneracy of the 1D orbitals into three groups of two (D_{xy} and $D_{x^2-y^2}$), two (D_{xz} and D_{yz}), and one (D_{z^2}) orbitals due to a crystal field splitting. In the minority states, after the P_z state, we found five unfilled 1D orbitals with similar degeneracies of the majority states (see Figure 7). The filling of majority and minority orbitals leads to $1S^21P^61D_\alpha^5$ orbitals resulting in a 5 μ_B magnetic moment in the VLi_8 cluster, which can mimic the situation in a manganese ion (Mn^{2+}) with a half-filled 3d shell. The Mn^{2+} ion has five electrons in excess of the closed-shell 18-electron argon configuration, as Figure 7 shows. Our finding of the VLi_8 cluster as a magnetic superatom can be classified into the previous discovery of superatoms in alkali metal clusters (VNa_8 and VCs_8) by Khanna and collaborators.[17]

We also made a detailed comparison between the VLi_8 and the corresponding pure Li_9 cluster. The lowest-energy isomer of the pure Li_9 cluster has a distorted squared-pyramidal structure similar to VLi_8. Figure 7 shows that the electronic shell structures of $1S^2$ and $1P^6$ are virtually unchanged as the V atom substitutes for the embedded Li atom, despite the slight loss of orbital degeneracy of the 1P state in the Li_9 cluster due to a lower symmetry. The delocalized electrons from the s valence states of Li atoms occupy the superatom S and P states. On the other hand, the localized electrons from the 3d V atom stabilize the magnetic moments. The present work shows that magnetic superatoms can be designed by appropriate combinations of localized and delocalized electrons in the valence space of a cluster. This also demonstrates that the electron shell closing model can be regarded as a simple but valid tool for explaining the structures and stabilities of metal clusters.

It is noticed from n = 8 that the geometries of the most stable VLi_n clusters are very similar, with an endohedral V atom in Li_n cages. We extended the orbital analysis to all of the VLi_n

dx.doi.org/10.1021/jp410489g | J. Phys. Chem. A 2013, 117, 13025−13036

clusters from the size of n = 9 to 13. The results are depicted in Figure 8. It is clear that all of the VLi_n (n = 9−13) clusters have superatomic orbitals. For example, the icosahedral VLi_{12} with perfect I_h symmetry can be viewed as another superatom with the superatomic configuration of $1S^21P^61D_\alpha^51D_\beta^4$ orbitals, as Figure 8 shows. Very recently, Cheng et al. reported that the pure lithium clusters can mimic the behavior of simple molecules in electronic shells, and they found that nonspherical clusters Li_{14}, Li_{10}, and Li_8 are analogues of F_2, N_2, and CH_4 molecules, respectively.[40] The geometries of Li_{14}, Li_{10}, and Li_8 clusters reported by Cheng et al. are consistent with the lowest-energy structures obtained in our work, as shown in Figure 1. This indicates that both pure lithium clusters and 3d TM impurity encapsulated lithium clusters hold strong tendency of forming superatoms.

Inspired by the result of doping a V atom in a Li_8 host to yield the most robust magnetic superatom among the above superatoms, we further extended studies to the situation of encapsulating other TM atoms (TM = Sc, Ti, V, Cr, Mn, Fe, Co, Ni, Cu, and Zn) in a Li_8 cage to examine the universality of the stability and magnetic properties. Our optimizations show that the lowest-energy structures of all $TMLi_8$ clusters are found to be a square antiprism of eight Li atoms with an endohedral TM atom, except for $ScLi_8$, which is a distorted square antiprism in C_{2v} symmetry with a Sc atom in the bottom of one square. Figure 9 gives the magnetic trends of $TMLi_8$

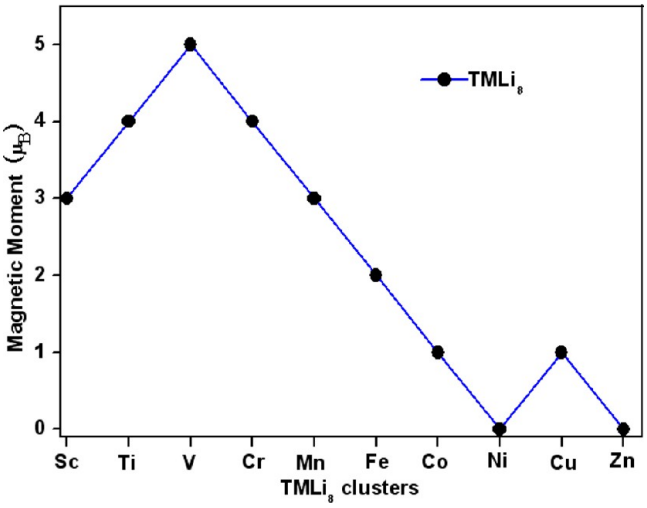

Figure 9. Magnetic trends of $TMLi_8$ (TM = Sc, Ti, V, Cr, Mn, Fe, Co, Ni, Cu, and Zn) clusters for the lowest-energy structures.

clusters as a function of the TM atom. It can be seen that there is a maximum value at VLi_8 with 5 μ_B, and the magnetic moment decreases successively on both sides of the VLi_8 cluster.

The thermodynamic stability of the ground-state structure of VLi_8 is also confirmed by using the Born−Oppenheimer molecular dynamics simulation implemented in the DMOL3 code at room temperature (T = 300 K). Our molecular dynamics simulation lasted for 4 ps, and the structure was monitored during this time. Each step in the molecular dynamics simulation was 0.4 fs long. We show that the D_{4d} symmetry structure of VLi_8 is stable. As shown in Figure 10, the relative potential energy remains unchanged within the time of the dynamic simulation.

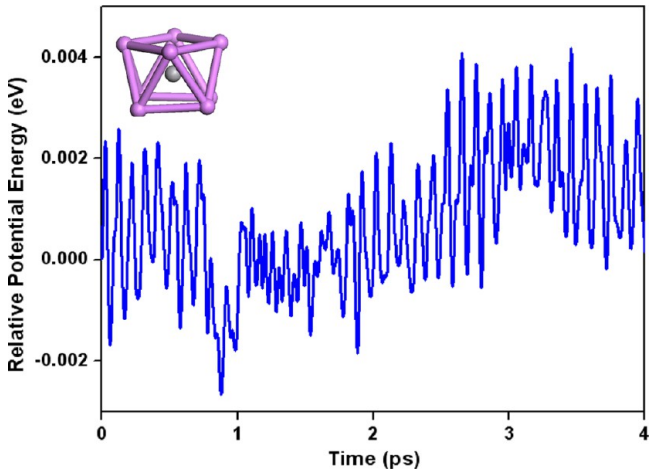

Figure 10. Relative potential energy (eV) of the VLi_8 structure during 4 ps of molecular dynamics simulation.

4. CONCLUSIONS

To find possible magnetic superatoms, a systematic study of geometrical structures, growth-pattern behaviors, relative stabilities, and electronic and magnetic properties of vanadium impurity doped Li_n (n = 1−13) clusters has been carried out via relativistic all-electron DFT with the generalized gradient approximation. Small VLi_n clusters exhibit extraordinary size-dependent properties. A single Li-atom-capped structure of the VLi_{n-1} cluster is a dominant growth pattern, while a cage-like structure happens when $n \geq 8$ and evolves toward an icosahedral shape with successive lithium atoms.

VLi_n clusters are found to be more stable in structural stability and tunable in magnetism than their corresponding pure Li_{n+1} clusters. Following the electronic and magnetic properties, the VLi_8 cluster is identified as a magnetic superatom with a jellium sphere electronic structure and a robust magnetic moment of 5 μ_B. Moreover, we found that magnetic superatoms exist in VLi_n clusters with an endohedral V atom from the size of n = 8 to 13. Taking the stability, tunable magnetic moment, and rich lithium environment of the VLi_n clusters into consideration, the VLi_n cluster superatoms show potential applications in spin-controllable energy storage electronics. The electronics will possess both magnetic properties as well as self-powering merits. We hope that the present work of a cluster superatom combining magnetism and stable features will serve as the starting point for further experimental synthesis and functionalization of such magnetic energy storage materials.

AUTHOR INFORMATION

Corresponding Authors

*E-mail: yhluo@ecust.edu.cn (Y.L.).
*E-mail: wei.cao@oulu.fi (W.C.).

Notes

The authors declare no competing financial interest.

ACKNOWLEDGMENTS

This work is financially supported partly by the National Natural Science Foundation of China (Grant No. 11204079 and 11304096), by the Natural Science Foundation of Shanghai (Grant No. 12ZR1407000), and the Fundamental Research Funds for the Central Universities (No. WM1214043). The Strategic Grant of Oulu University is also acknowledged.

REFERENCES

(1) Kroto, H. W.; Heath, J. R.; O'Brien, S. C.; Curl, R. F.; Smalley, R. E. C_{60}: Buckminsterfullerene. *Nature* **1985**, *318*, 162−163.

(2) Baev, A.; Samoc, M.; Prasad, P. N.; Krykunov, M.; Autschbach, J. A Quantum Chemical Approach to the Design of Chiral Negative Index Materials. *Opt. Express* **2007**, *15*, 5730−5741.

(3) Fromen, M. C.; Morillo, J.; Casanove, M. J.; Lecante, P. Structure and Chemical Order in Co−Rh Nanoparticles. *Europhys. Lett.* **2006**, *73*, 885−891.

(4) Haruta, M. Size- and Support-Dependency in the Catalysis of Gold. *Catal. Today* **1997**, *36*, 153−166.

(5) Khanna, S. N.; Jena, P. Atomic Clusters: Building Blocks for a Class of Solids. *Phys. Rev. B* **1995**, *51*, 13705−13716.

(6) Ashman, C.; Khanna, S. N.; Liu, F.; Jena, P.; Kaplan, T.; Mostoller, M. $(BAl_{12})Cs$: A Cluster-Assembled Solid. *Phys. Rev. B* **1997**, *55*, 15868−15873.

(7) Kumar, V.; Kawazoe, Y. Metal-Encapsulated Icosahedral Superatoms of Germanium and Tin with Large Gaps: $Zn@Ge_{12}$ and $Cd@Sn_{12}$. *Appl. Phys. Lett.* **2002**, *80*, 859−861.

(8) Neukermans, S.; Janssen, E.; Chen, Z. F.; Silverans, R. E.; Schleyer, P. v. R.; Lievens, P. Extremely Stable Metal-Encapsulated $AlPb_{10}^+$ and $AlPb_{12}^+$ Clusters: Mass-Spectrometric Discovery and Density Functional Theory Study. *Phys. Rev. Lett.* **2004**, *92*, 163401−163900.

(9) Bergeron, D. E.; Castleman, A. W., Jr.; Morisato, T.; Khanna, S. N. Formation of $Al_{13}I^-$: Evidence for the Superhalogen Character of Al_{13}. *Science* **2004**, *304*, 84−87.

(10) Reveles, J. U.; Khanna, S. N.; Roach, P. J.; Castleman, A. W., Jr. Multiple Valence Superatoms. *Proc. Natl. Acad. Sci. U.S.A.* **2006**, *103*, 18405−18410.

(11) Castleman, A. W., Jr.; Khanna, S. N.; Sen, A.; Reber, A. C.; Qian, M.; Davis, K. M.; Peppernick, S. J.; Ugrinov, A.; Merritt, M. D. From Designer Clusters to Synthetic Crystalline Nanoassemblies. *Nano Lett.* **2007**, *7*, 2734−2741.

(12) Hartig, J.; Stößer, A.; Hauser, P.; Schnöckel, H. A Metalloid $[Ga_{23}\{N(SiMe_3)_2\}_{11}]$ Cluster: The Jellium Model Put to Test. *Angew. Chem., Int. Ed.* **2007**, *46*, 1658−1662.

(13) Jung, J.; Kim, H.; Han, Y. K. Can an Electron-Shell Closing Model Explain the Structure and Stability of Ligand-Stabilized Metal Clusters? *J. Am. Chem. Soc.* **2011**, *133*, 6090−6095.

(14) Bergeron, D. E.; Roach, P. J.; Castleman, A. W., Jr.; Jones, N. O.; Khanna, S. N. Al Cluster Superatoms as Halogens in Polyhalides and as Alkaline Earths in Iodide Salts. *Science* **2005**, *307*, 231−234.

(15) Walter, M.; Akola, J.; Lopez-Acevedo, O.; Jadzinsky, P. D.; Calero, G.; Ackerson, C. J.; Whetten, R. L.; Grönbeck, H.; Häkkinen, H. A Unified View of Ligand-Protected Gold Clusters as Superatom Complexes. *Proc. Natl. Acad. Sci. U.S.A.* **2008**, *105*, 9157−9162.

(16) De Heer, W. A. The Physics of Simple Metal Clusters: Experimental Aspects and Simple Models. *Rev. Mod. Phys.* **1993**, *65*, 611−676.

(17) Reveles, J. U.; Clayborne, P. A.; Reber, A. C.; Khanna, S. N.; Pradhan, K.; Sen, P.; Pederson, M. R. Designer Magnetic Superatoms. *Nat. Chem.* **2009**, *1*, 310−315.

(18) He, H.; Pandey, R.; Reveles, J. U.; Khanna, S. N.; Karna, S. S. Highly Efficient (Cs_8V) Superatom-Based Spin-Polarizer. *Appl. Phys. Lett.* **2009**, *95*, 192104/1−192104/3.

(19) Castleman, A. W., Jr.; Khanna, S. N. Clusters, Superatoms, and Building Blocks of New Materials. *J. Phys. Chem. C* **2009**, *113*, 2664−2675.

(20) Chauhan, V.; Medel, V. M.; Reveles, J. U.; Khanna, S. N.; Sen, P. Shell Magnetism in Transition Metal Doped Calcium Superatom. *Chem. Phys. Lett.* **2012**, *528*, 39−43.

(21) Medel, V. M.; Reveles, J. U.; Islam, M. F.; Khanna, S. N. Robust Magnetic Moments on Impurities in Metallic Clusters: Localized Magnetic States in Superatoms. *J. Phys. Chem. A* **2013**, *117*, 4297−4303.

(22) Zhang, X. X; Wang, Y.; Wang, H. P.; Lim, A.; Gantefoer, G.; Bowen, K. H.; Reveles, J. U.; Khanna, S. N. On the Existence of Designer Magnetic Superatoms. *J. Am. Chem. Soc.* **2013**, *135*, 4856−4861.

(23) Benichou, E.; Allouche, A. R.; Aubert-Frecon, M.; Antoine, R.; Broyer, M.; Dugourd, P.; Rayane, D. Experimental and Theoretical Investigations of Ionization Potentials and Structures of Mixed Sodium Lithium Clusters. *Chem. Phys. Lett.* **1998**, *290*, 171−179.

(24) Brock, L. R.; Knight, A. M.; Reddic, J. E.; Pilgrim, J. S.; Duncan, M. A. Photoionization Spectroscopy of Ionic Metal Dimers: LiCu and LiAg. *J. Chem. Phys.* **1997**, *106*, 6268−6278.

(25) Sarkas, H. W.; Arnold, S. T.; Hendricks, J. H.; Slager, V. L.; Bowen, K. H. Characterization of the $X^2\Sigma_u^+$ State of $^7Li_2^-$ via Negative Ion Photoelectron Spectroscopy. *Z. Phys. D* **1994**, *29*, 209−212.

(26) Bréchignac, C.; Busch, H.; Cahuzac, P.; Leygnier, J. Dissociation Pathways and Binding Energies of Lithium Clusters from Evaporation Experiments. *J. Chem. Phys.* **1994**, *101*, 6992−7002.

(27) Kornath, A.; Kaufmann, A.; Zoermer, A.; Ludwig, R. Raman Spectroscopic Investigation of Small Matrix-Isolated Lithium Clusters. *J. Chem. Phys.* **2003**, *118*, 6957−6963.

(28) Muz, İ.; Atiş, M.; Canko, O.; Yıldırım, E. K. Ab Initio Search for Global Minimum Structures of Neutral and Anionic Hydrogenated Li_5 Clusters. *Chem. Phys.* **2013**, *418*, 14−21.

(29) Yepes, D.; Kirk, S. R.; Jenkins, S.; Restrepo, A. Structures, Energies and Bonding in Neutral and Charged Li Microclusters. *J. Mol. Model.* **2012**, *18*, 4171−4189.

(30) Gardet, G.; Rogemond, F.; Chermette, H. Density Functional Theory Study of Some Structural and Energetic Properties of Small Lithium Clusters. *J. Chem. Phys.* **1996**, *105*, 9933−9947.

(31) Wheeler, S. E.; Sattelmeyer, K. W.; Schleyer, P. v. R.; Schaefer, H. F.; Wu, C. H. Binding Energies of Small Lithium Clusters (Li_n) and Hydrogenated Lithium Clusters (Li_nH). *J. Chem. Phys.* **2004**, *120*, 4683−4689.

(32) Jones, R. O.; Lichtenstein, A. I.; Hutter, J. Density Functional Study of Structure and Bonding in Lithium Clusters Li_n and Their Oxides Li_nO. *J. Chem. Phys.* **1997**, *106*, 4566−4574.

(33) Tai, T. B.; Nhat, P. V.; Nguyen, M. T.; Li, S.; Dixon, D. A. Electronic Structure and Thermochemical Properties of Small Neutral and Cationic Lithium Clusters and Boron-Doped Lithium Clusters: $Li_n^{0/+}$ and $Li_nB^{0/+}$ (n = 1−8). *J. Phys. Chem. A* **2011**, *115*, 7673−7686.

(34) Blanc, J.; Bonačić-Koutecký, V.; Broyer, M.; Chevaleyre, J.; Dugourd, P.; Koutecký, J.; Scheuch, C.; Wolf, J.; Wöste, L. Evolution of the Electronic-Structure of Lithium Clusters between Four and Eight Atoms. *J. Chem. Phys.* **1992**, *96*, 1793−1809.

(35) Sung, M. W.; Kawai, R.; Weare, J. H. Packing Transitions in Nanosized Li Clusters. *Phys. Rev. Lett.* **1994**, *73*, 3552−3555.

(36) Fournier, R.; Cheng, J. B. Y.; Wong, A. Theoretical Study of the Structure of Lithium Clusters. *J. Chem. Phys.* **2003**, *119*, 9444−9454.

(37) Goel, N.; Gautam, S.; Dharamvir, K. Density Functional Studies of Li_N and Li_N^+ (N = 2−30) Clusters: Structure, Binding and Charge Distribution. *Int. J. Quantum Chem.* **2012**, *112*, 575−586.

(38) Alexandrova, A. N.; Boldyrev, A. I. Search for the $Li_n^{0/+1/-1}$ (n = 5−7) Lowest-Energy Structures Using the Ab Initio Gradient Embedded Genetic Algorithm (GEGA). Elucidation of the Chemical Bonding in the Lithium Clusters. *J. Chem. Theory Comput.* **2005**, *1*, 566−580.

(39) Alexandrova, A. N.; Boldyrev, A. I.; Li, X.; Sarkas, H. W.; Hendricks, J. H.; Arnold, S. T.; Bowen, K. H. Lithium Cluster Anions: Photoelectron Spectroscopy and ab Initio Calculations. *J. Chem. Phys.* **2011**, *134*, 044322/1−044322/8.

(40) Cheng, L. J.; Yang, J. L. Communication: New Insight into Electronic Shells of Metal Clusters: Analogues of Simple Molecules. *J. Chem. Phys.* **2013**, *138*, 141101/1−141101/4.

(41) Jiang, Z. Y.; Lee, K. H.; Li, S. T.; Chu, S. Y. Structures and Charge Distributions of Cationic and Neutral Li_nX_m (X = Na and K). *Int. J. Mass Spectrom.* **2006**, *253*, 104−111.

(42) Pérez, J.; Flórez, E.; Hadad, C.; Fuentealba, P.; Restrepo, A. Stochastic Search of the Quantum Conformational Space of Small Lithium and Bimetallic Lithium−Sodium Clusters. *J. Phys. Chem. A* **2008**, *112*, 5749−5755.

(43) Deshpande, M. D.; Kanhere, D. G. Density-Functional Study of Structural and Electronic Properties of Na_nLi and Li_nNa ($1 \leq n \leq 12$) Clusters. *Phys. Rev. A* **2002**, *65*, 033202/1−033202/6.
(44) Baruah, T.; Kanhere, D. G. Topological Study of Charge Densities of Impurity Doped Small Li Clusters. *Phys. Rev. A* **2001**, *63*, 063202/1−063202/8.
(45) Deshpande, M.; Dhavale, A.; Zope, R. R.; Chacko, S.; Kanhere, D. G. Ground-State Geometries and Stability of Impurity Doped Clusters: Li_nBe and Li_nMg (n = 1−12). *Phys. Rev. A* **2000**, *62*, 063202/1−063202/7.
(46) Meden, A.; Mavri, J.; Bele, M.; Pejovnik, S. Dissolution of Boron in Lithium Melt. *J. Phys. Chem.* **1995**, *99*, 4252−4260.
(47) Li, Y.; Wu, D.; Li, Z. R.; Sun, C. C. Structural and Electronic Properties of Boron-Doped Lithium Clusters: Ab Initio and DFT Studies. *J. Comput. Chem.* **2007**, *28*, 1677−1684.
(48) Li, Y.; Liu, Y. J.; Wu, D.; Li, Z. R. Evolution of the Structures and Stabilities of Boron-Doped Lithium Cluster Cations: Ab Initio and DFT Studies. *Phys. Chem. Chem. Phys.* **2009**, *11*, 5703−5710.
(49) Nguyen, K. A.; Lammertsma, K. Structure, Bonding, and Stability of Small Boron−Lithium Clusters. *J. Phys. Chem. A* **1998**, *102*, 1608−1614.
(50) Nguyen, K. A.; Srinivas, G. N.; Hamilton, T. P.; Lammertsma, K. Stability of Hyperlithiated Borides. *J. Phys. Chem. A* **1999**, *103*, 710−715.
(51) Tai, T. B.; Nguyen, M. T. Thermochemical Properties, Electronic Structure and Bonding of Lithium-Doped Boron Clusters (B_nLi, n = 1−8) and Their Anions. *Chem. Phys.* **2010**, *375*, 35−45.
(52) Tai, T. B.; Nguyen, M. T. The High Stability of Boron-Doped Lithium Clusters Li_5B, $Li_6B^{\pm}$ and Li_7B: A Case of the Phenomenological Shell Model. *Chem. Phys. Lett.* **2010**, *489*, 75−80.
(53) Boldyrev, A. I.; Simons, J.; Schleyer, P. v. R. Ab Initio Study of the Electronic Structures of Lithium Containing Diatomic Molecules and Ions. *J. Chem. Phys.* **1993**, *99*, 8793−8804.
(54) Boldyrev, A. I.; Gonzales, N.; Simons, J. Periodicity and Peculiarity in 120 First- and Second-Row Diatomic Molecules. *J. Phys. Chem.* **1994**, *98*, 9931−9944.
(55) Nemukhin, A. V.; Almlöf, J.; Heiberg, A. Potential Curves for BLi and BLi^+. *Chem. Phys. Lett.* **1980**, *76*, 601−603.
(56) Tai, T. B.; Nhat, P. V.; Nguyen, M. T. Structure and Stability of Aluminium Doped Lithium Clusters ($Li_nAl^{0/+}$, n = 1−8): A Case of the Phenomenological Shell Model. *Phys. Chem. Chem. Phys.* **2010**, *12*, 11477−11486.
(57) Kuma, V. $Al_{10}Li_8$: A Magic Compound Cluster. *Phys. Rev. B* **1999**, *60*, 2916−2920.
(58) Guo, X. Q.; Podloucky, R.; Freeman, A. J. Phase Stability and Bonding Characteristics of Li-Rich Al−Li Intermetallic Compounds: Al_2Li_3 and Al_4Li_9. *Phys. Rev. B* **1990**, *42*, 10912−10923.
(59) Chacko, S.; Kanhere, D. G. Evolution of the Structural and Bonding Properties of Aluminum−Lithium Clusters. *Phys. Rev. A* **2004**, *70*, 023204/1−023204/9.
(60) Akola, J.; Manninen, M. Aluminum−Lithium Clusters: First-Principles Simulation of Geometries and Electronic Properties. *Phys. Rev. B* **2002**, *65*, 245424/1−245424/8.
(61) Cheng, H. P.; Barnett, R. N.; Landman, U. Energetics and Structures of Aluminum−Lithium Clusters. *Phys. Rev. B* **1993**, *48*, 1820−1824.
(62) Lee, M. S.; Gowtham, S.; He, H.; Lau, K. C.; Pan, L.; Kanhere, D. G. Geometry, Electronic Properties, and Thermodynamics of Pure and Al-Doped Li Clusters. *Phys. Rev. B* **2006**, *74*, 245412/1−245412/6.
(63) Tai, T. B.; Nguyen, M. T. Electronic Structure and Thermochemical Properties of Silicon-Doped Lithium Clusters $Li_nSi^{0/+}$, n = 1−8: New Insights on Their Stability. *J. Comput. Chem.* **2012**, *33*, 800−809.
(64) Lievens, P.; Thoen, P.; Bouckaert, S.; Bouwen, W.; Vanhoutte, W.; Weidele, H.; Silverans, R. E.; Vazquez, A. N.; Schleyer, P. v. R. Ionization Potentials of Hypervalent Li_nC ($2 \leq n \leq 10$). *Eur. Phys. J. D* **1999**, *9*, 289−295.
(65) Lievens, P.; Thoen, P.; Bouckaert, S.; Bouwen, W.; Vanhoutte, F.; Weidele, H.; Silverans, R. E. Evidence for Size-Dependent Electron Delocalization in the Ionization Potentials of Lithium Monocarbide Clusters. *Chem. Phys. Lett.* **1999**, *302*, 571−576.
(66) Ivanic, J.; Marsden, C. J. Novel, Remarkably Stable Polylithiated Carbon Species: CLi_8, CLi_{10}, and CLi_{12}. *J. Am. Chem. Soc.* **1993**, *115*, 7503−7504.
(67) Kudo, H. Observation of Hypervalent CLi_6 by Knudsen-Effusion Mass Spectrometry. *Nature* **1992**, *355*, 432−434.
(68) Schleyer, P. v. R.; Wurthwein, E. U.; Kaufman, E.; Lark, T.; Pople, J. A. CLi_5, CLi_6, and the Related Effectively Hypervalent First-Row Molecules, $CLi_{5-n}H_n$, and $CLi_{6-n}H_n$. *J. Am. Chem. Soc.* **1983**, *105*, 5930−5932.
(69) Joshi, K.; Kanhere, D. G. Ab Initio Investigation of Electronic Structure, Equilibrium Geometries, and Finite-Temperature Behavior of Sn-Doped Li_n Clusters. *Phys. Rev. A* **2002**, *65*, 043203/1−043203/7.
(70) Shetty, S.; Pal, S.; Kanhere, D. G. A Study of Electronic and Bonding Properties of Sn Doped Li_n Clusters and Aluminum Based Binary Clusters through Electron Localization Function. *J. Chem. Phys.* **2003**, *118*, 7288−7296.
(71) Joshi, K.; Kanhere, D. G. Finite Temperature Behavior of Impurity Doped Lithium Cluster, Li_6Sn. *J. Chem. Phys.* **2003**, *119*, 12301−12307.
(72) Gopakumar, G.; Lievens, P.; Nguyen, M. T. Interaction of Triatomic Germanium with Lithium Atoms: Electronic Structure and Stability of Ge_3Li_n Clusters. *J. Phys. Chem. A* **2007**, *111*, 4353−4361.
(73) Ngan, V. T.; Haeck, J. H.; Le, H. T.; Gopakumar, G.; Lievens, P.; Nguyen, M. T. Experimental Detection and Theoretical Characterization of Germanium-Doped Lithium Clusters Li_nGe (n = 1−7). *J. Phys. Chem. A* **2009**, *113*, 9080−9091.
(74) DMOL3 is a density functional theory program distributed by Accelrys, Inc. See also: Delley, B. An All-Electron Numerical Method for Solving the Local Density Functional for Polyatomic Molecules. *J. Chem. Phys.* **1990**, *92*, 508−517.
(75) Doye, J. P. K.; Wales, D. J. Global Optimization by Basin-Hopping and the Lowest Energy Structures of Lennard-Jones Clusters Containing up to 110 Atoms. *J. Phys. Chem. A* **1997**, *101*, 5111−5116.
(76) Wales, D. J.; Scheraga, H. A. Global Optimization of Clusters, Crystals, and Biomolecules. *Science* **1999**, *285*, 1368−1372.
(77) Becke, A. D. Density-Functional Exchange-Energy Approximation with Correct Asymptotic Behavior. *Phys. Rev. A* **1988**, *38*, 3098−3100.
(78) Lee, C.; Yang, W.; Parr, R. G. Development of the Colle−Salvetti Correlation-Energy Formula into a Functional of the Electron Density. *Phys. Rev. B* **1988**, *37*, 785−789.
(79) Perdew, J. P.; Burke, K.; Ernzerhof, M. Generalized Gradient Approximation Made Simple. *Phys. Rev. Lett.* **1996**, *77*, 3865−3868.
(80) Perdew, J. P.; Wang, Y. Accurate and Simple Analytic Representation of the Electron−Gas Correlation Energy. *Phys. Rev. B* **1992**, *45*, 13244−13249.
(81) Nhat, P. V.; Nguyen, M. T. Trends in Structural, Electronic and Energetic Properties of Bimetallic Vanadium−Gold Clusters Au_nV with n = 1−14. *Phys. Chem. Chem. Phys.* **2011**, *13*, 16254−16264.
(82) Jena, P.; Khanna, S. N.; Rao, B. K. *Physics and Chemistry of Small Metal Clusters*; Jena, P., Khanna, S. N., Rao, B. K., Eds.; Plenum Press: New York, 1987.
(83) Frisch, M. J.; Trucks, G. W.; Schlegel, H. B.; Scuseria, G. E.; Robb, M. A.; Cheeseman, J. R.; Scalmani, G.; Barone, V.; Mennucci, B.; Petersson, G. A.; et al. *Gaussian 09*, revision B. 01; Gaussian, Inc.: Wallingford, CT, 2010.